Climate Dynamics (2023) 60:785–796
https://doi.org/10.1007/s00382-022-06346-6

Comparison of southward shift mechanisms of equatorial westerly anomalies between EP and CP El Niño

Yuhan Gong[1] · **Tim Li**[1,2]

Received: 6 December 2021 / Accepted: 8 May 2022 / Published online: 7 June 2022

Abstract
A composite analysis of observational data reveals that maximum westerly anomalies associated with both the EP and CP El Niños shift southward to 5° S during their mature phase (boreal winter), with different zonal locations. A zonal momentum budget analysis indicates that leading factors to cause the southward shift of the zonal wind anomaly for both EP and CP El Niño composites are anomalous pressure gradient force and anomalous meridional advection, while anomalous Coriolis force has an opposite effect. The difference in the longitudinal locations arises from the zonal shift of maximum SST anomaly centers between EP and CP El Niño. Prior to northern winter, the westerly anomaly for both types of El Niño is approximately symmetric about the equator. The advection by the climatological mean cross-equatorial wind leads to initial southward shift of the maximum westerly and subsequent development of an antisymmetric mode through a moisture-convection-circulation feedback and a wind-evaporation-SST feedback. An EOF analysis of the tropical Pacific surface wind field indicates that both the first and second leading modes are important in contributing to the southward shift of the maximum westerly anomaly with distinctive longitudinal locations for CP and EP El Niño.

Keywords Southward shift of westerly anomalies · Zonal momentum budget · Meridional advection by the climatological mean flow · Development of an antisymmetric mode

1 Introduction

The El Niño-Southern Oscillation (ENSO), as the most dominant interannual variability in the globe, is characterized by a marked sea surface temperature anomaly (SSTA) and associated wind and precipitation anomalies in the equatorial Pacific (Rasmusson and Carpenter 1982; Cane and Zebiak 1985; Philander 1990; McPhaden et al. 1998). The seasonal phase locking is one of the most robust and defining characteristics of ENSO evolution. ENSO typically starts to develop in boreal spring or summer and reaches its mature phase in boreal winter (Rasmusson and Carpenter 1982; Philander 1990). The cause of this phase locking is attributed to the annual modulation of the stability of ENSO due to the seasonal variation of the background state of the tropical Pacific (Philander et al. 1984). There are various theories to explain this seasonal modulation, including but not limited to the season-dependent coupled instability in eastern equatorial Pacific (Li 1997; Li and Hsu 2017), equatorial easterly forcing associated with an anomalous low-level anticyclone in tropical western North Pacific (Wang et al. 1999, 2000; An and Wang 2001), or a season-dependent cloud-radiation feedback (Neelin et al. 2000; Dommenget and Yu 2016).

An interesting characteristic of ENSO evolution is that during its mature phase, the maximum zonal wind anomaly in the equatorial central Pacific (CP) tends to shift southward away from the equator, while the SSTA center is approximately symmetric about the equator (Harrison 1987). This southward shift decreases the amplitude of the wind anomaly at the equator, which may affect its development and favor a faster phase transition (Harrison and Vecchi 1999;

✉ Tim Li
timli@hawaii.edu

[1] Key Laboratory of Meteorological Disaster, Ministry of Education (KLME)/Joint International Research Laboratory of Climate and Environmental Change (ILCEC)/ Collaborative Innovation Center On Forecast and Evaluation of Meteorological Disasters (CIC-FEMD), Nanjing University of Information Science and Technology, Nanjing, China

[2] Department of Atmospheric Sciences, International Pacific Research Center, School of Ocean and Earth Science and Technology, University of Hawaii at Manoa, Honolulu, HI 96822, USA

Vecchi and Harrison 2003; Spencer 2004; Lengaigne et al. 2006; McGregor et al. 2012). It has been shown that the southward shift of the zonal wind anomaly could alter the discharge process of the warm water volume at the equator (McGregor et al. 2012, 2013). Abellán and McGregor (2016), Abellán et al. (2017) showed that models with better performance of the southward shifting could simulate ENSO phase locking more realistically.

Various studies attempted to understand the causes of the westerly shift. For instance, it was suggested that the southward shift might be attributed to the equatorially asymmetric mean state as maximum mean SST and the South Pacific convergence zone (SPCZ) are located south of the equator (Vecchi and Harrison 2003; Spencer 2004; Lengaigne et al. 2006; Vecchi 2006; McGregor et al. 2012). Such an asymmetry might favor the development of anomalous convection south of the equator. However, such a hypothesis requires further observational, theoretical and modeling support. Using a simple atmospheric model, McGregor et al. (2012) suggested that a weakening of boundary layer Ekman damping favored the southward shift of the westerly anomaly, but such a weakening is not observed in a momentum budget diagnosis (Gong and Li 2021). Recently Gong and Li (2021) proposed a mechanism that involves two-step processes. The maximum westerly anomaly was initially pushed southward by anomalous advection of the climatological mean cross-equatorial flow. It was further amplified by unstable development of an antisymmetric mode through both the moisture-convection-circulation and wind-evaporation-SST (WES) feedbacks (Xie and Philander 1994; Li and Philander 1996).

However, the study of Gong and Li (2021) focused on the contrast of El Niño and La Niña composite without the separation of EP and CP El Niño types. The distinctive SSTA patterns between CP and EP type El Niño have been studied in great deal (e.g., Larkin and Harrison 2005; Ashok et al. 2007; Kug et al. 2009; Yeh et al. 2009; Kao and Yu 2009). For CP (EP) El Niño, maximum SSTA centers are located in central (eastern) Pacific. It has been shown that the El Niño type is to a large extent controlled by the inter-decadal mean state (McPhaden et al. 2011; Chung and Li 2013; Xiang et al. 2013; Capotondi et al. 2015; Hu and Fedorov 2018). The EP El Niño dominated during the period of 1979–1998 while the CP El Niño dominated during the period of 1999–2014. Besides, the temporal evolution of CP and EP El Niño also shows a distinctive feature (Chen and Li 2021).

There are controversial views on the meridional shift of the zonal wind anomaly during the mature phase of CP and EP El Niño. For instance, McGregor et al. (2013) suggested that the extent of meridional shift of the zonal wind anomaly depended on the El Niño magnitude. The wind shift might play a role in the termination of a strong El Niño but not of a moderate El Niño or a La Niña (Lengaigne et al. 2006; McGregor et al. 2013), because the wind shift for a moderate El Niño or a La Niña is weak. Zhang et al. (2015) suggested that the zonal wind shift was only presented for EP El Niño but not for CP El Niño or La Niña. This is in contrast with Gong and Li (2021), who pointed out that there was a clear southward shift of the zonal wind anomaly during La Niña mature winter.

The controversial views above motivated the current study. In this paper, we intend first to examine the observed wind evolution patterns for the EP and CP El Niño groups respectively and then to investigate the physical mechanisms responsible for the zonal wind shift. The remainder of this paper is organized as follow. Section 2 introduces the datasets and methods. Section 3 illustrates the observed evolution features of the zonal wind anomaly patterns for the two types of El Niño. A zonal momentum budget analysis is followed to reveal mechanisms responsible for the wind difference in Sect. 4. A discussion on possible cause of the controversy views is given in the Sect. 5. Finally, a conclusion is given in Sect. 6.

2 Data and methods

a. Data

The primary data used in this study are daily reanalysis fields including geopotential height (hgt), horizontal and vertical velocity(u, v, ω), precipitation (pr) and specific humidity (q) from the European Centre for Medium-Range Weather Forecasts (ECMWF) interim (ERA-Interim; Dee and Uppala 2009) and SST product from the HadISST version 1.1 (Rayner et al. 2003). The daily reanalysis data are used in the zonal momentum budget diagnosis. The horizontal resolution of the atmospheric reanalysis data from ERA-Interim is 0.5°× 0.5°, and the horizontal resolution of SST is 1°× 1°. The current analysis covers the period of 1979–2018.

b. Methods

Most of previous studies that defined a CP El Niño were based on the longitudinal location of maximum SSTA center during its mature phase, neglecting the SSTA temporal evolution during its onset and developing stage. Here we follow the work by Xiang et al. (2013), who defined a CP El Niño based on the SSTA location in both the developing and mature phases. Four CP El Niño cases were picked up since 1979. These CP El Niño years are in 1994/1995, 2002/2003, 2004/2005, 2009/2010. It is worth mentioning that these four cases are common CP El Niño events among different definitions from different authors (Ashok et al. 2007; Kug et al. 2009; Yeh et al. 2009; McPhaden et al. 2011; Wang et al. 2019). Disputable CP El Niño events include those in 1986, 1987, 1991 and 2006, which exhibited a mixed feature as the SSTA center appeared in EP in some period and moved

to CP in other period during the El Niño life cycle. To compare the aforementioned CP El Niño group with the EP El Niño group, three robust EP El Niño events (1982/1983, 1997/1998, 2015/2016) are selected. It is worth noting that Paek et al. (2017) considered 2015/2016 as a strong mixed El Niño not a pure EP-type El Niño due to its westward SSTA location. However, according to Wang et al. (2019), despite its more westward location than 1997/1998, its maximum SSTA still always locates in eastern Pacific. The wind response of 2015/2016 is examined and it is more like the "pure" El Niño. Thus, this event is still deemed as EP El Niño in our research to increase the sample size.

To understand the fundamental mechanism for the equatorial asymmetry, we diagnose the antisymmetric zonal momentum budget following Gong and Li (2021). Each variable is decomposed into a symmetric and an antisymmetric component relative to the equator. Following Li (1997), any variables except the meridional wind field (v) can be decomposed into

$$var_s(y) = \frac{var(y) + var(-y)}{2} \tag{1}$$

$$var_a(y) = \frac{var(y) - var(-y)}{2} \tag{2}$$

where y denotes latitude, subscripts s and a represent the symmetric and antisymmetric component respectively. For the meridional wind field (v), its equatorially symmetric and antisymmetric components are defined as:

$$v_s(y) = \frac{v(y) - v(-y)}{2} \tag{3}$$

$$v_a(y) = \frac{v(y) + v(-y)}{2} \tag{4}$$

To investigate specific physical processes that cause the equatorial asymmetry of the zonal wind anomaly, an antisymmetric zonal wind tendency equation using daily data is diagnosed. The antisymmetric zonal momentum budget equation can be written as follows:

$$\left(\frac{\partial u}{\partial t}\right)'_a = -\left(u\frac{\partial u}{\partial x}\right)'_a - \left(v\frac{\partial u}{\partial y}\right)'_a - \left(\omega\frac{\partial u}{\partial p}\right)'_a + fv'_a - \left(\frac{\partial \varphi}{\partial x}\right)'_a + (F_x)'_a \tag{5}$$

where u, v, ω denote the 3-dimensional (3D) wind, $\frac{\partial u}{\partial t}$ denotes the zonal wind tendency, $-u\frac{\partial u}{\partial x}$, $-v\frac{\partial u}{\partial y}$, and $-\omega\frac{\partial u}{\partial p}$ are 3D advection terms, f is the Coriolis parameter, φ denotes the geopotential height, F_x denotes the apparent momentum sink term that is calculated using daily raw data and original zonal momentum equation following the idea of Yanai et al. (1973). A prime denotes the interannual anomaly, and subscript a represents the antisymmetric component of each term. Each variable in the nonlinear advection terms may be decomposed into a climatological mean component and an interannual anomaly, to reveal the mean flow effect.

3 Observed features of the westerly shift during EP and CP El Niño events

The composite evolution patterns of anomalous SST and zonal wind fields for EP and CP El Niño groups are shown in Fig. 1. In northern fall (Fig. 1a, d), the westerly anomalies are quasi-symmetric with a maximum center right on the equator for both EP and CP El Niño composites. Then the westerly center moves to the south of the equator for both types of El Niño in boreal winter (Fig. 1b, e). The extent of the meridional shift is similar, about 5° in latitude. It is worth noting that the westerly anomaly center displays a farther eastward location for EP El Niño group with its maximum center at about 160° W, while the westerly center appears at about 180° for CP El Niño composite. The westerly anomaly weakens quickly in subsequent spring in the CP El Niño composite, while the westerly anomaly can still be seen in EP El Niño composite (Fig. 1c, f).

Figure 2 shows the vertical structure of the anomalous zonal wind field averaged over the maximum center region for two types of El Niño. Considering their different zonal locations, the zonal wind anomaly is averaged over 170° E–150° W for EP El Niño and over 160° E–160° W for CP El Niño. The result clearly indicates that the maximum westerly anomaly is confined in lower troposphere and shifted to near 5° S in DJF for both EP and CP El Niño composite, despite of a weaker intensity for CP El Niño.

Given that the anomalous westerly for both types of El Niño is confined in the lower troposphere, in the following we will focus on the momentum budget analysis within the 1000–700 hPa layer. Figure 3 illustrates the horizontal patterns of vertically (1000–700 hPa) integrated zonal wind field and its antisymmetric tendency in boreal winter. The vertically averaged zonal wind fields (Fig. 3a, c) resemble the surface wind anomaly fields shown in Fig. 1a, d, with a southward shift of the maximum westerly in central Pacific (green boxes in Fig. 3a, c). The bottom panel of Fig. 3 shows the 1000–700 hPa integrated antisymmetric zonal wind tendency field. A positive (negative) zonal wind tendency appears in general to the south (north) of the equator over the green box longitudes. In the following we will diagnose the antisymmetric zonal wind budget in the green boxes to reveal factors that generate and maintain maximum westerly anomalies south of the equator.

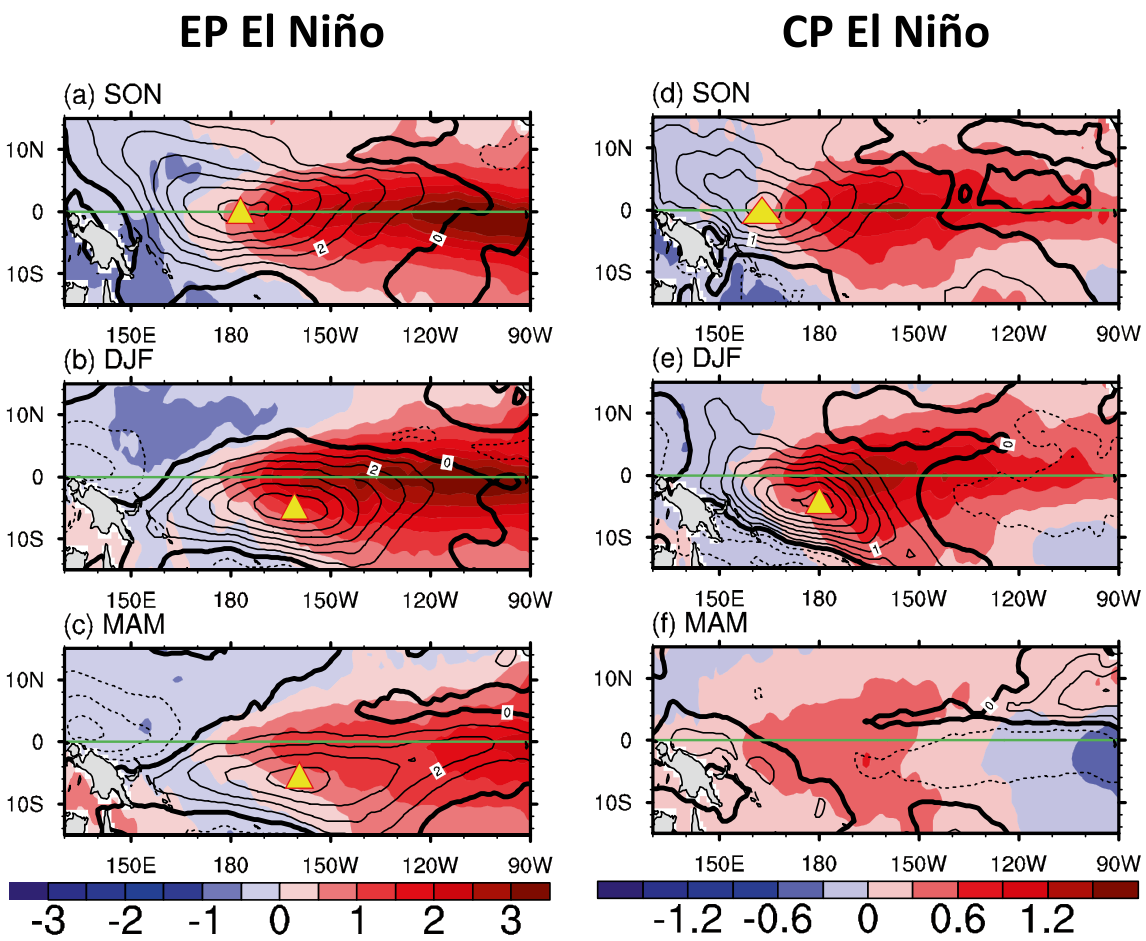

Fig. 1 The composite evolution patterns of anomalous SST (shading; °C) and 10-m zonal wind (contour; m s^{-1}) fields for **a**–**c** EP El Niño and **d**–**f** CP El Niño from SON to MAM. The interval for **a**–**c** is 1 m s^{-1} and for **d**–**f** is 0.5 m s^{-1}. The triangles mark the center of maximum zonal wind anomalies

4 Antisymmetric zonal momentum budgets for EP and CP El Niño composites

To understand specific physical processes that cause the southward shift of the maximum westerly anomaly for EP and CP El Niños, the antisymmetric zonal momentum budget is conducted based on Eq. 5. The budget results averaged over the green boxes are displayed in Fig. 4. The value of each term represents the contrast of zonal wind tendency between Southern Hemisphere (SH) and Northern Hemisphere (NH). A positive value means that this term contributes westerly acceleration in SH, and thus is responsible for the generation and maintenance of the maximum westerly anomaly south of the equator. For EP El Niño (Fig. 4a), the two leading positive terms are anomalous meridional advection $[-\left(v\frac{\partial u}{\partial y}\right)_a']$ and anomalous pressure gradient force $[-\left(\frac{\partial \varphi}{\partial x}\right)_a']$, followed by the Coriolis force (fv_a'). The budget result of CP El Niño (Fig. 4b) is similar to that of EP El Niño, with the same leading terms, namely, anomalous meridional advection and anomalous pressure gradient force. However, anomalous Coriolis force term has an opposite sign for CP El Niño, implying that this term tends to decelerate the maximum westerly south of the equator. The apparent momentum sink term $[(F_x)_a']$ has strong negative effect for both EP and CP El Niño.

The horizontal distributions of the three leading terms are shown in Fig. 5. The meridional advection term is in general positive in the green box, whereas the pressure gradient force term is positive primarily to the west of the box, as a minimum anomalous pressure center is located to the east of the box. The Coriolis force term has a positive (negative) value to the northeast (southwest) of the box, and its average value depends on relative strength of the positive and negative values. For EP El Niño, the positive value dominates, and for CP El Niño, the negative value in the southwest of the box prevails (Fig. 5c, f).

By further separating the anomalous meridional advection term into the advection of the anomalous zonal wind by

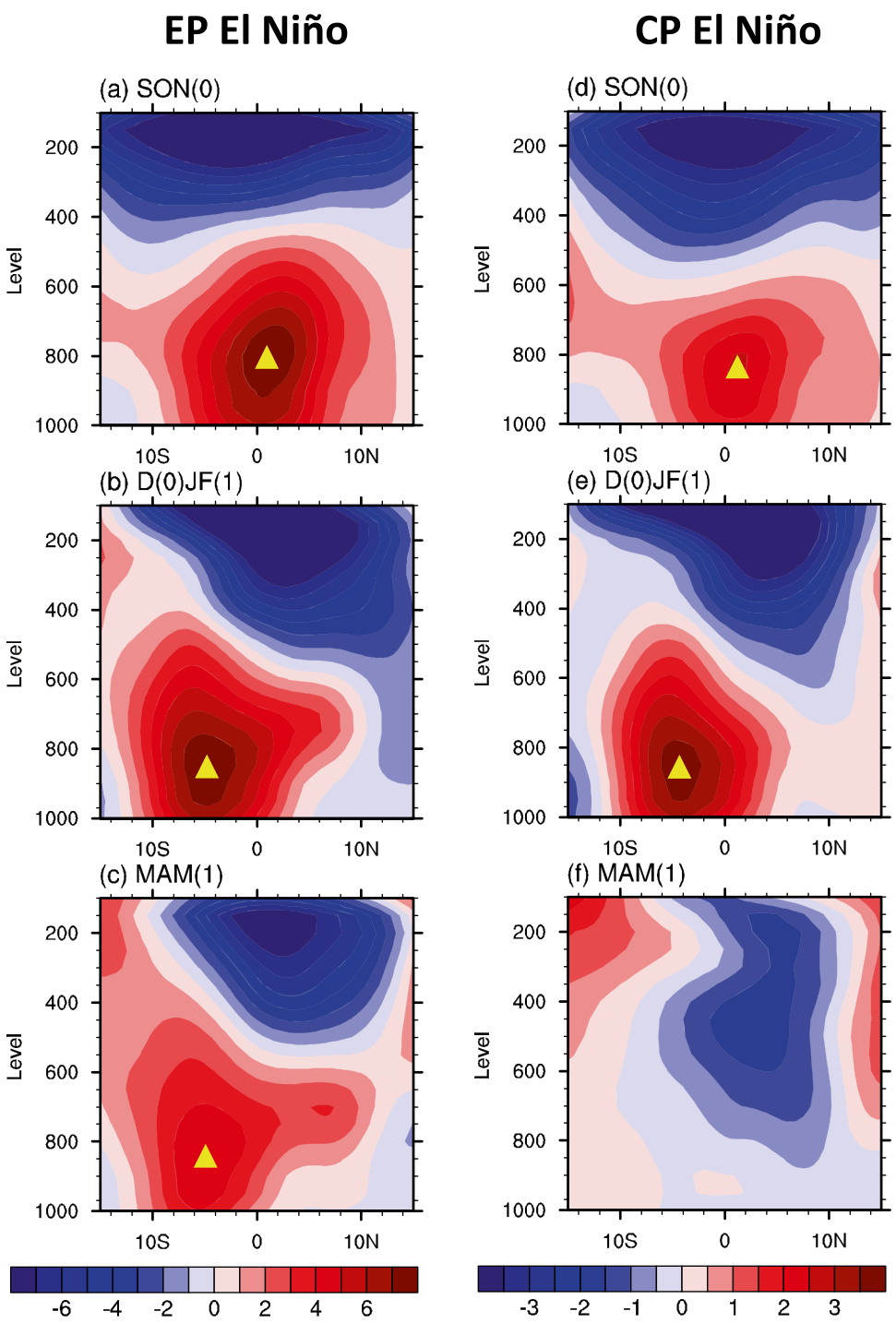

Fig. 2 Vertical-latitude cross sections of anomalous zonal wind fields averaged at **a–c** 170° E–150° W from SON to MAM for EP El Niño and **d–f** 160° E–160° W for CP El Niño. The triangle marks the center of maximum zonal wind anomalies

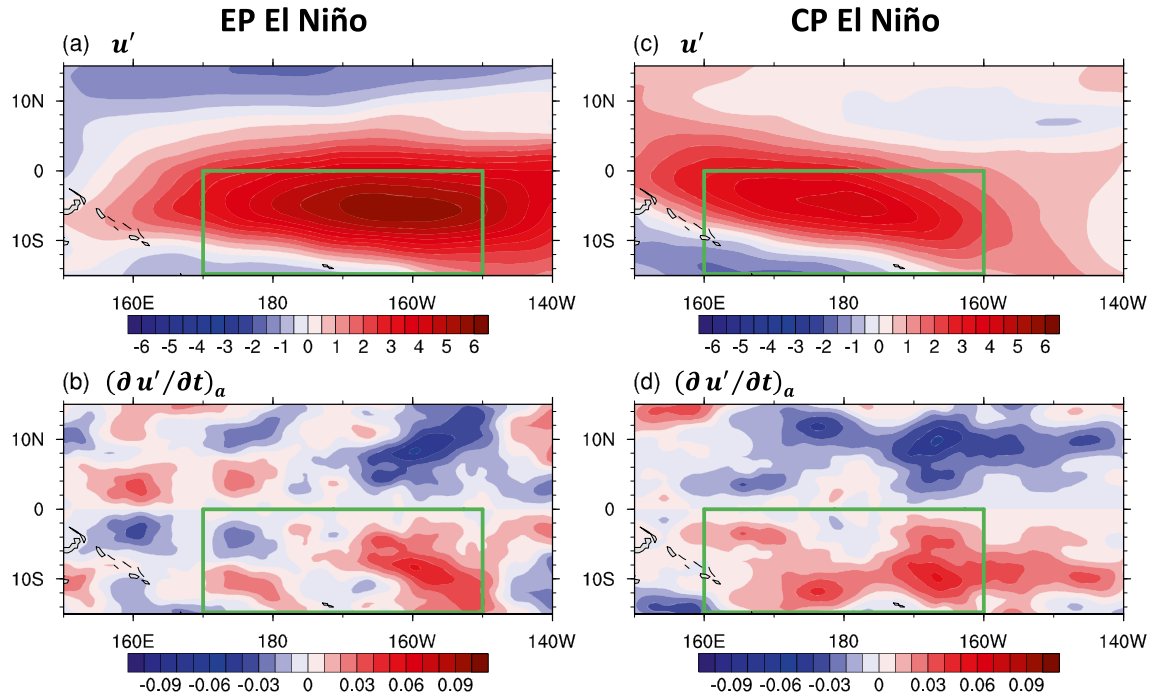

Fig. 3 Composite horizontal patterns of anomalous zonal wind (u', m s.$^{-1}$) and antisymmetric zonal wind tendency $[\left(\frac{\partial u'}{\partial t}\right)_a]$ averaged over 1000-700 hPa in D(0)JF(1) for **a**, **b** EP El Niño and **c**, **d** CP El Niño. The green boxes denote the maximum westerly regions for EP El Niño (0°–15° S, 170° E–150° W) and CP El Niño (0°–15° S, 160° E–160° W)

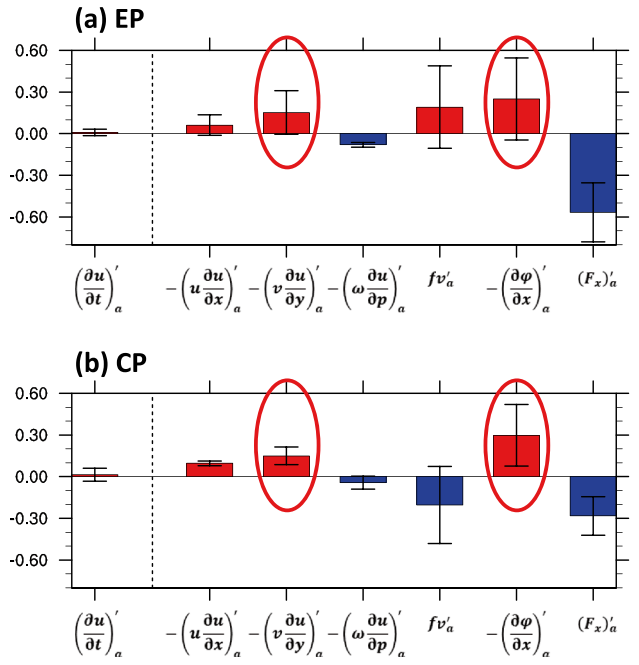

Fig. 4 The values of each of the antisymmetric zonal momentum budget terms (unit: 10^{-5} m s^{-2}) in D(0)JF(1) for **a** EP El Niño and **b** CP El Niño, averaged over the green boxes shown in Fig. 3. The whiskers indicate the standard deviations among cases

the mean climatological flow and the advection of the mean zonal wind by anomalous meridional flow, Gong and Li (2021) found that the most important contributor of the meridional advection term is $-\overline{v}_a\frac{\partial u'_s}{\partial y}$. which represents the advection of symmetric component of the anomalous zonal wind by the antisymmetric component of the climatological meridional wind. Following this approach, we decompose the meridional advection term for both the CP and EP El Niño composites and found that the same term $(-\overline{v}_a\frac{\partial u'_s}{\partial y})$ dominates. The physical interpretation of this term is straightforward. In northern winter there are pronounced climatological southward low-level cross-equatorial flows. The mean southerlies push the El Niño generated maximum westerly southward from the equator. The main difference between CP and EP El Niño lies on the longitudinal location of the maximum westerly. Compared to EP El Niño, the maximum westerly appears further toward the west in CP El Niño (Fig. 6), because of its westward location of the SSTA center. As a consequence, the meridional advection tends to shift its effect westward in CP El Niño compared to that in EP El Niño.

The westward shift feature for CP El Niño is also seen in the development of an antisymmetric unstable mode, as

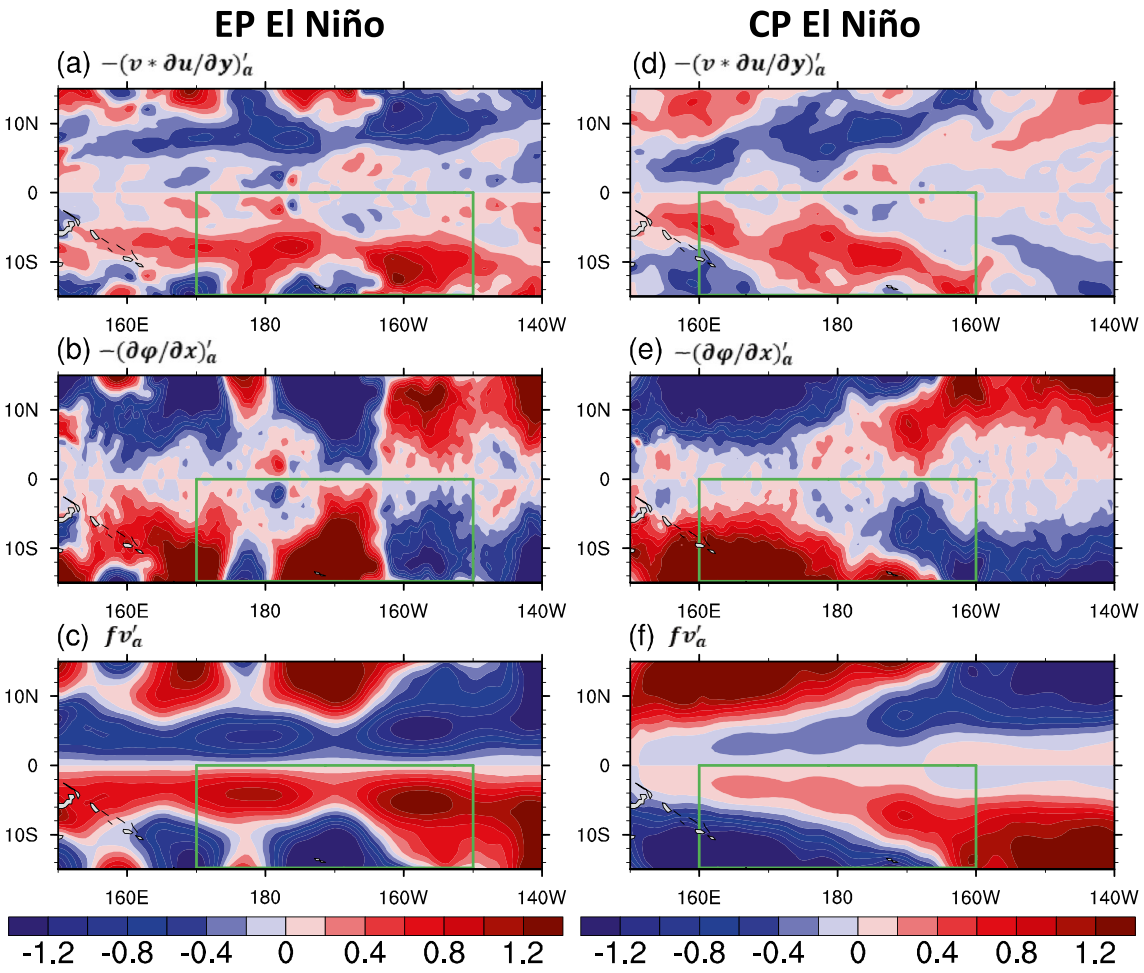

Fig. 5 The horizontal patterns of three leading terms $[-\left(v\frac{\partial u}{\partial y}\right)'_a, -\left(\frac{\partial \varphi}{\partial x}\right)'_a$ and $fv'_a]$ (unit: 10^{-5} m s^{-2}) in the antisymmetric zonal momentum budget analysis in D(0)JF(1) for **a**–**c** EP El Niño and **d**, **e** CP El Niño

shown in Fig. 7. The antisymmetric mode manifests the asymmetry of precipitation along with asymmetric pressure, moisture, SST and wind. It was argued that the southward shift of the maximum westerly during El Niño may promote the development of an antisymmetric mode through various positive feedback processes (moisture-convection-circulation feedback and wind-evaporation-SST feedback; Gong and Li 2021). After the maximum westerly anomalies shift southward by the meridional advection, it advects high mean moisture and moisture enthalpy eastward from the warm pool, increasing the atmospheric convection in situ. The enhanced convection induces cross-equatorial flow and promotes the development of an antisymmetric mode. Meanwhile, the westerly anomalies decrease the mean trade wind, leading to a decreased surface evaporation and thus a warmer SSTA in SH. The warm SSTA can further strengthen the antisymmetric mode development. Figure 7 confirms that the longitudinal location of the antisymmetric mode differs between CP and EP El Niño. The maximum centers of the anomalous SST, precipitation, geopotential height and moisture fields all display westward in the former compared to those in the latter (Fig. 7). Such a longitudinal location difference is primarily caused by the SSTA pattern diversity between CP and EP El Niño.

The relatively weaker intensity of the antisymmetric mode for CP El Niño compared to EP El Niño is possibly attributed to the difference of the westerly anomaly intensity at the equator. The wind difference is further caused by

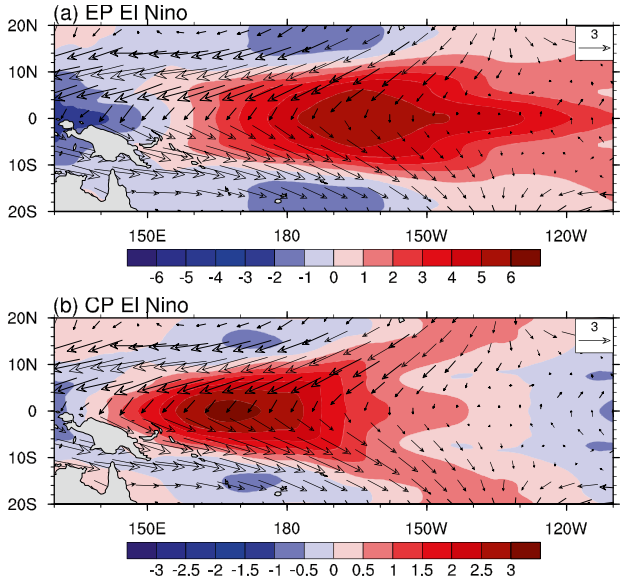

Fig. 6 Horizontal patterns of the antisymmetric climatological mean wind ($\overline{u}_a$, $\overline{v}_a$; vector, m s^{-1}) in boreal winter (DJF) and the symmetric component of the anomalous zonal wind (u'_s, shading, m s^{-1}) in D(0)JF(1) averaged over 1000–700 hPa for **a** EP El Niño and **b** CP El Niño composite

the distinctive SSTA intensities between the two types of El Niño. Accompanying with an anomalous low pressure center south of the equator (Fig. 7f), anomalous southward cross-equatorial winds dominate the central Pacific while anomalous northerlies appear in the southwestern Pacific (Fig. 7e). This explains why the Coriolis force displays a positive (negative) zonal wind tendency to the northeast (southwest) of the green box shown in Fig. 5f.

5 Discussion

In this section we would like to discuss what causes the discrepancy between the current work and the previous study of Zhang et al. (2015) regarding the southward shift of the westerly anomaly during the CP El Niño. As seen from Figs. 1 and 2, there is a clear southward shift in DJF in the CP El Niño composite. Zhang et al. (2015), however, suggested that the zonal wind shift only occurs during EP El Niño, not CP El Niño. The conclusion by Zhang et al. (2015) was based on an EOF analysis of the surface wind anomaly field in the tropical Pacific, following McGregor et al. (2012) and Stuecker et al. (2013). The main assumption of Zhang et al. (2015) is that the leading EOF mode represents a symmetric wind pattern while the second EOF mode represents an asymmetric wind pattern so that the southward shift is only represented by the second mode. By composing the reconstructed wind anomalies based on the second EOF mode, Zhang et al. (2015) got a weak southward shift for CP El Niño composite. This prompted them to conclude that the CP El Niño does not exhibit a southward shift.

To demonstrate the importance of both the EOF modes in representing the observed southward shift characteristics, we follow exactly the same methodology applied in Zhang et al. (2015). To remove the influence of other factors, the same ENSO cases are selected and the same dataset are used below. Figure 8 illustrates the two leading EOF modes of the surface wind anomaly field in the tropical Pacific. Note that both the modes exhibit a clear equatorial asymmetry. While the maximum westerly anomaly center associated with EOF1 appears 10° west of the dateline, the maximum westerly anomaly center associated with EOF2 is located at 20° east of the dateline. In addition, there are pronounced equatorial easterly anomalies in the western Pacific associated with an anomalous anticyclone there. The pronounced difference in the longitudinal location of the maximum westerly center between the two EOF patterns, as demonstrated later, is critical in reconstructing the anomalous wind patterns associated with CP and EP El Niño.

Figure 9 shows the reconstructed wind anomaly patterns for EP and CP El Niño composite, based on the first principal component (PC1), the second principal component (PC2) and combined PC1 and PC2 respectively. Obviously, the zonal wind anomaly fields reconstructed based on PC1 show a clear southward shift of the maximum westerly for both EP and CP El Niño, with the maximum zonal wind center around 3° S (Fig. 9a, d). The reconstructed zonal wind anomaly based on PC2 is strong for EP El Niño but very weak for CP El Niño (Fig. 9b, e). This is because the observed westerly anomaly center for CP El Niño appears west of the dateline (Fig. 1e) while the westerly anomaly center of EOF2 appears at east of the dateline (around 160° W) (Fig. 8b). Therefore, the CP El Niño induced westerly anomaly center has an approximately 90° phase difference with the EOF2 wind center. This is why the CP El Niño wind pattern can hardly be projected onto EOF2. The reconstructed wind fields based on both the EOF modes, on the other hand, show a clear southward shift for both the EP and CP El Niño composites (Fig. 9c, f), with distinctive longitudinal locations. Such reconstructed wind patterns resemble the observed composites (Fig. 1b, e).

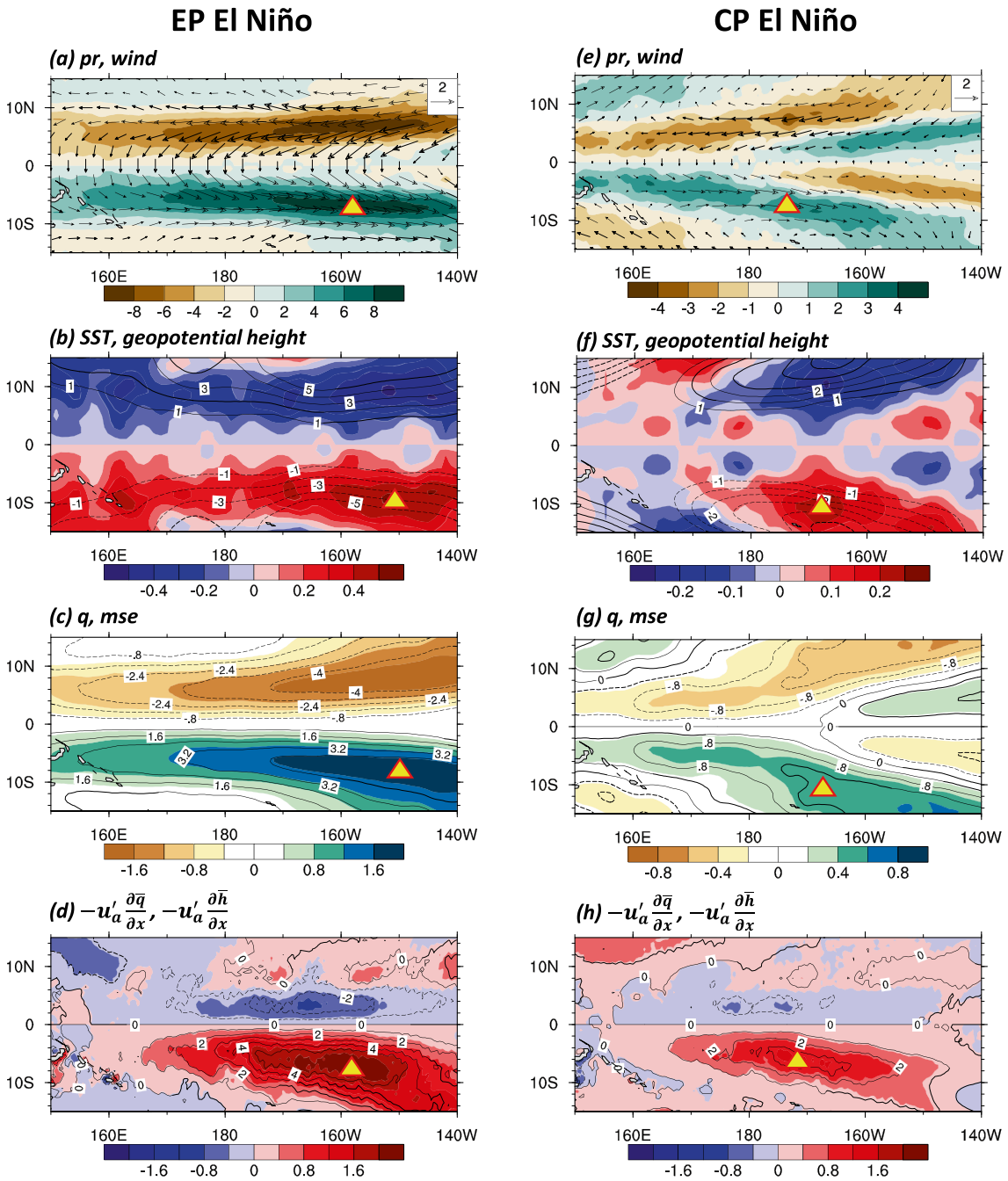

Fig. 7 The composite patterns of the antisymmetric mode during EP El Niño (left) and CP El Niño (right) in D(0)JF(1). Variables shown are (**a**, **e**) anomalous precipitation (shading, mm day^{-1}) and average wind over 1000 hPa-700 hPa (vector, m s^{-1}), **b**, **f**) anomalous SST (shading, K) and geopotential height averaged over 1000–700 hPa (contour, interval for **b**: 1 gpm, interval for **f**: 0.5 gpm), and **c**, **g** anomalous specific humidity (shading, g kg^{-1}) and moist static energy (MSE) [contour interval: 0.4×10^3 W m^2; solid (dashed) line indicates positive (negative) value] averaged over 1000 hPa-700 hPa, where $MSE = C_pT + L_vq + \varnothing$. **d**, **h** The horizontal distribution of anomalous moisture advection ($-u'_a\frac{\partial\bar{q}}{\partial x}$, shading, 10^9 s^{-1}) and anomalous moist enthalpy ($h = C_pT + L_vq$) advection ($-u'_a\frac{\partial\bar{h}}{\partial x}$, contour, 10^3 W m^2 s^{-1}) averaged over 1000–700 hPa. Triangles at each panel mark the anomaly centers

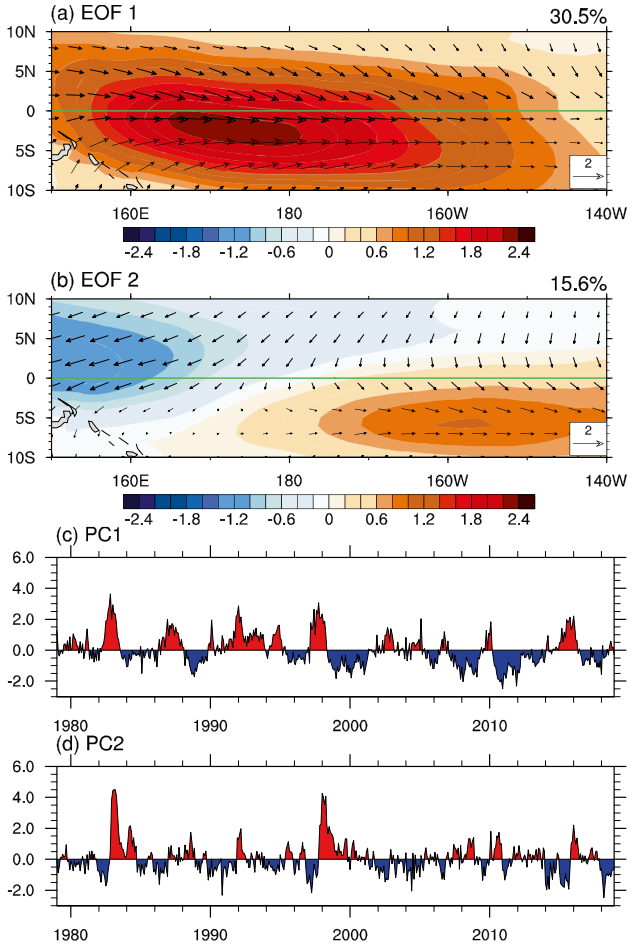

Fig. 8 **a**, **b** The horizontal patterns and **c**, **d** corresponding normalized PC time series of the leading two EOF modes of 10-m wind anomalies (vector, m s^{-1}) in the tropical Pacific (10°–10° S, 100° E-80° W). The color shading in (**a**, **b**) denotes the anomalous zonal wind field (m s^{-1})

Thus, based on the EOF analysis above, we demonstrate that a southward shift of the westerly anomaly does exist in CP El Niño composite and that the previous study that used the same longitudinal zone (140° E–140° W) average neglected the marked longitudinal asymmetry between the EP and CP El Niño and severely underestimated the southward shift in the CP composite. Because of the use of the wider longitudinal domain, a maximum anomalous precipitation center appears north rather than south of the equator in CP El Niño composite (Fig. 10 of Zhang et al., 2015), which is inconsistent with the anomalous wind pattern (e.g., Fig. 7e). Therefore, to fully represent the southward shift characteristics for both the CP and EP El Niño, one needs to consider both the longitudinal and latitudinal asymmetries of the zonal wind anomaly field.

6 Conclusion

A composite analysis of the observational data reveals that the southward shift of the maximum westerly anomalies occurs during the mature phase (DJF) of both EP and CP El Niño. The extent of the southward shift for the two types of El Niño is similar, near 5° in latitude (Figs. 1, 2). However, the longitudinal locations of the southward shift differ during EP and CP El Niño. The maximum westerly center appears at 160° W for EP El Niño composite and west of the dateline for CP El Niño composite (Fig. 1). In addition, the intensity of the shifted westerly anomalies appears weaker for CP El Niño compared to EP El Niño.

Physical mechanisms for the southward shift are examined through an antisymmetric zonal momentum budget analysis. For both the CP and EP El Niño, dominant processes that generate and maintain the antisymmetric zonal wind tendency arise from the advection of the El Niño generated symmetric zonal wind anomaly by the southward cross-equatorial climatological mean flow and an anomalous pressure gradient force linking to the development of an antisymmetric mode. The main difference between the two types of El Niño lies on the anomalous Coriolis force (Fig. 4), which is controlled by anomalous circulation pattern south of the equator.

The distinctive longitudinal locations of the southward shift between the CP and EP El Niño are primarily attributed to the different zonal locations of the maximum SSTA center at the equator. Compared to EP El Niño, the maximum SSTA center shifts westward in CP El Niño, and so is the maximum westerly at the equator. As the season progresses from boreal fall to winter, maximum solar radiation shifts to SH, leading to a strengthened SPCZ and a southward climatological cross-equatorial flow in western-central Pacific, which advects the anomalous westerly southward. The zonal location of the westerly anomaly center is primarily determined by the location of initial westerly maximum at the equator. As indicated by Gong and Li (2021), an antisymmetric mode is further developed due to anomalous moisture advection caused by the shifted westerly anomaly. The antisymmetric mode is further magnified through a moisture-convection-circulation feedback and a wind-evaporation-SST feedback (Gong and Li 2021). The current observational analysis illustrates distinctive longitudinal locations for the antisymmetric mode between two types of El Niño, as seen from anomalous precipitation, wind, moisture and geopotential height fields (Fig. 7). They are about 15° in longitude apart. Such a zonal asymmetry is consistent with the longitudinal difference in the maximum equatorial westerly field between CP and EP El Niño (Fig. 6).

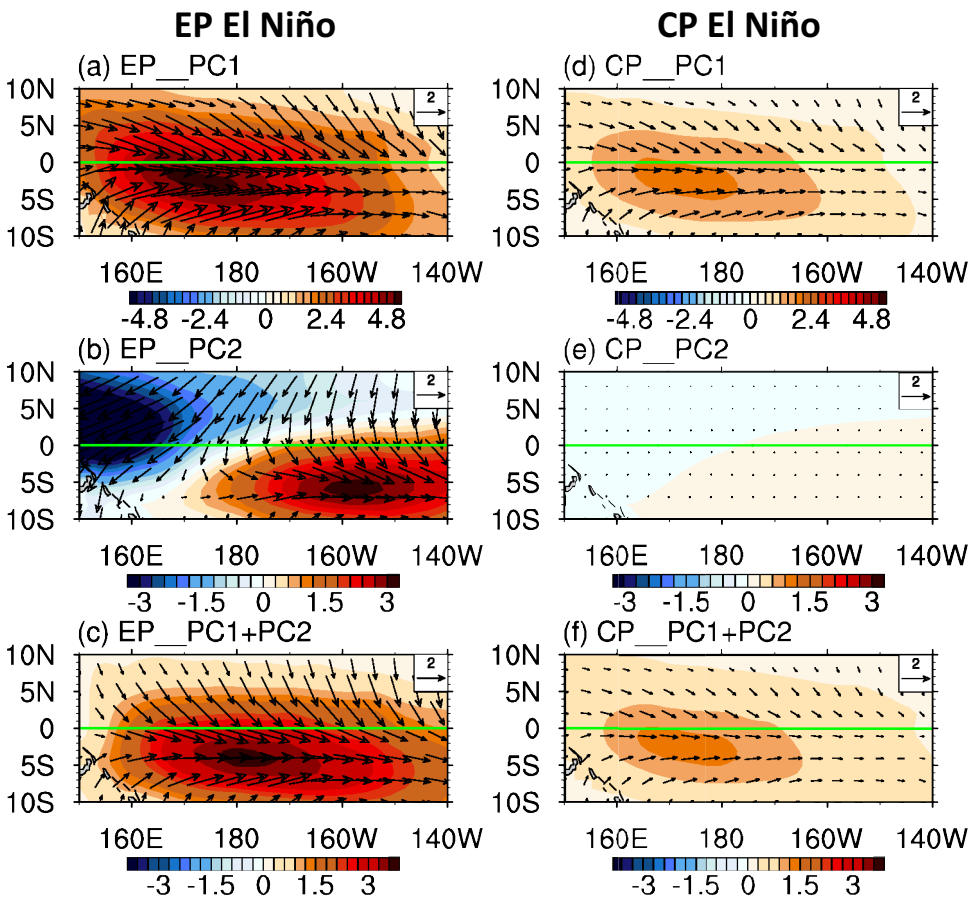

Fig. 9 The reconstructed 10-m wind anomaly fields (vector, m s^{-1}) in D(0)JF(1) for EP El Niño (left) and CP El Niño (right) derived based on PC1 (top panel), PC2 (middle panel) and combined PC1 and PC2 (bottom panel). The color shading denotes the anomalous zonal wind field (m s^{-1})

Acknowledgements This work was supported by National Natural Science Foundation of China (42088101), NSF (AGS-2006553) and NOAA (NA18OAR4310282). This is SOEST contribution number 11522, IPRC contribution number 1569, and ESMC contribution 380.

Data availability statement The HadISST dataset is available at: http://www.metoffice.gov.uk/hadobs/. ERA-Interim data were downloaded at: http://www.ecmwf.int/en/research/climate-reanalysis/era-interim.

Declarations

Conflict of interest The authors have not disclosed any competing interests.

References

Abellán E, McGregor S (2016) The role of the southward wind shift in both the seasonal synchronization and duration of ENSO events. Clim Dyn 47:509–527

Abellán E, McGregor S, England MH (2017) Analysis of the Southward Wind Shift of ENSO in CMIP5 models. J Clim 30:2415–2435

An S-I, Wang B (2001) Mechanisms of Locking of the El Niño and La Niña Mature Phases to Boreal Winter. J Clim 14:2164–2176

Ashok K, Behera SK, Rao SA, Weng H, Yamagata T (2007) El Niño Modoki and its possible teleconnection. J Geophys Res 112:C11007. https://doi.org/10.1029/2006JC003798

Cane MA, Zebiak SE (1985) A theory for El Niño and the Southern Oscillation. Science 228:1085–1087

Capotondi A, Wittenberg AT, Newman M, Di Lorenzo E, Yu JY, Braconnot P, Cole P, Dewitte B, Giese B, Guilyardi E, Jin FF, Karnauskas K, Kirtman B, Lee T, Schneider N, Xue Y, Yeh SW (2015) Understanding ENSO diversity. Bull Amer Met Soc 96(6):921–938

Chen M, Li T (2021) ENSO evolution asymmetry: EP versus CP El Niño. Clim Dyn 56:3569–3579

Chung PH, Li T (2013) Interdecadal Relationship between the Mean State and El Niño Types. J Clim 26:361–379

Dee DP, Uppala S (2009) Variational bias correction of satellite radiance data in the ERA-Interim reanalysis. Q J R Meteorol Soc 135:1830–1841

Dommenget D, Yu Y (2016) The seasonally changing cloud feedbacks contribution to the ENSO seasonal phase-locking. Clim Dynam 47:3661–3672

Gong Y, Li T (2021) Mechanism for Southward Shift of Zonal Wind Anomalies during the Mature Phase of ENSO. J Clim 34:8897–8911

Harrison DE (1987) Monthly mean island surface winds in the central tropical Pacific and El Niño events. Mon Wea Rev 115:3133–3145

Harrison DE, Vecchi GA (1999) On the termination of El Niño. Geophys Res Lett 26:1593–1596

Hu S, Fedorov AV (2018) Cross-equatorial winds control El Niño diversity and change. Nat Clim Change 8:798–802

Kao H-Y, Yu J-Y (2009) Contrasting Eastern-Pacific and Central-Pacific types of ENSO. J Clim 22:615–632

Kug J-S, Jin F-F, An S-I (2009) Two types of El Niño events: cold tongue El Niño and warm pool El Niño. J Clim 22:1499–1515
Larkin NK, Harrison DE (2005) Global seasonal temperature and precipitation anomalies during El Nino autumn and winter. Geophys Res Lett 32:L16705. https://doi.org/10.1029/2005GL022860
Lengaigne M, Boulanger J-P, Menkes C, Spencer H (2006) Influence of the seasonal cycle on the termination of El Niño events in a coupled general circulation model. J Clim 19:1850–1868
Li T (1997) Air–sea interactions of relevance to the ITCZ: Analysis of coupled instabilities and experiments in a hybrid coupled GCM. J Atmos Sci 54:134–147
Li T, Hsu PC (2017) ENSO dynamics. Fundamentals of tropical climate dynamics. Springer International Publishing, Cham, p 236
Li T, Philander SGH (1996) On the annual cycle of the eastern equatorial Pacific. J Clim 9:2986–2998
McGregor S, Timmermann A, Schneider N, Stuecker MF, England MH (2012) The effect of the South Pacific convergence zone on the termination of El Niño events and the meridional asymmetry of ENSO. J Clim 25:5566–5586
McGregor S, Ramesh N, Spence P, England MH, McPhaden MJ, Santoso A (2013) Meridional movement of wind anomalies during ENSO events and their role in event termination. Geophys Res Lett 40:749–754
McPhaden M, Busalacchi A, Cheney R, Donguy J-R, Gage K, Halpern D, Ji M, Meyers PJG, Mitchum G, Niiler P, Picaut J, Reynolds R, Smith N, Takeuchi K (1998) The tropical ocean-global atmosphere observing system: a decade of progress. J Geophys Res 103:14169–14240
McPhaden MJ, Lee T, McClurg D (2011) El Niño and its relationship to changing background conditions in the tropical Pacific Ocean. Geophys Res Lett 38:L15709. https://doi.org/10.1029/2011GL048275
Neelin JD, Jin F-F, Syu H-H (2000) Variations in ENSO Phase Locking. J Clim 13:2570–2590
Paek H, Yu J-Y, Qian C (2017) Why were the 2015/2016 and 1997/1998 extreme El Niños different? Geophys Res Lett 44:1848–1856
Philander SG (1990) El Niño, La Niña, and the southern oscillation. Academic Press, London, p 289
Philander SG, Yamagata T, Pacanowski R (1984) Unstable air-sea interactions in the tropics. J Atmos Sci 41:604–613
Rasmusson EM, Carpenter TH (1982) Variations in tropical sea surface temperature and surface wind fields associated with the Southern Oscillation/El Niño. Mon Weather Rev 110:354–384
Rayner N, Parker D, Horton E, Folland C, Alexander L, Powell D (2003) Global analyses of SST, sea ice and night marine air temperature since the late nineteenth century. J Geophys Res 108. https://doi.org/10.1029/2002JD002670
Spencer H (2004) Role of the atmosphere in seasonal phase locking of El Niño. Geophys Res Lett 31:L24104. https://doi.org/10.1029/2004GL021619
Stuecker MF, Timmermann A, Jin F-F, McGregor S, Ren H-L (2013) A combination mode of the annual cycle and the El Niño/Southern Oscillation. Nat Geosci 6:540–544
Vecchi GA (2006) The Termination of the 1997–98 El Niño. Part II: mechanisms of atmospheric change. J Clim 19:2647–2664
Vecchi GA, Harrison DE (2003) On the termination of the 2002–2003 El Niño event. Geophys Res Lett 30:1964. https://doi.org/10.1029/2003GL017564
Wang B, Wu R, Lukas R (1999) Roles of the Western North Pacific Wind Variation in Thermocline Adjustment and ENSO Phase Transition. J Meteorol Soc Japan 77:1–16
Wang B, Wu R, Fu X (2000) Pacific-East Asian teleconnection: how does ENSO affect East Asian Climate? J Clim 13:1517–1536
Wang B, Luo X, Yang YM, Sun W, Liu J (2019) Historical change of El Niño properties sheds light on future changes of extreme El Niño. Proc Natl Acad Sci U S A 116:22512–32251
Xiang B, Wang B, Li T (2013) A new paradigm for the predominance of standing Central Pacific Warming after the late 1990s. Clim Dyn 41:327–340
Xie S-P, Philander SGH (1994) A coupled ocean-atmosphere model of relevance to the ITCZ in the eastern Pacific. Tellus A 46:340–350
Yanai M, Esbensen S, Chu J-H (1973) Determination of bulk properties of tropical cloud clusters from large-scale heat and moisture budgets. J Atmos Sci 30:611–627
Yeh S-W, Kug J-S, Dewitte B, Kwon M-H, Kirtman BP, Jin F-F (2009) El Niño in a changing climate. Nature 461:511–514
Zhang W, Li H, Jin F-F, Stuecker MF, Turner AG, Klingaman NP (2015) The Annual-cycle modulation of meridional asymmetry in ENSO's atmospheric response and its dependence on ENSO zonal structure. J Clim 28:5795–5812